Energy 42 (2012) 213–223

Contents lists available at SciVerse ScienceDirect

Energy

journal homepage: www.elsevier.com/locate/energy

Comparison of the Organic Flash Cycle (OFC) to other advanced vapor cycles for intermediate and high temperature waste heat reclamation and solar thermal energy

Tony Ho*, Samuel S. Mao, Ralph Greif

Department of Mechanical Engineering, University of California-Berkeley, Etcheverry Hall, Berkeley, CA 94720, USA

ARTICLE INFO

Article history:
Received 27 August 2011
Received in revised form
22 February 2012
Accepted 24 March 2012
Available online 22 April 2012

Keywords:
Organic Rankine Cycle (ORC)
Solar thermal
Waste heat
Vapor cycle
Exergy analysis

ABSTRACT

The Organic Flash Cycle (OFC) is proposed as a vapor power cycle that could potentially improve the efficiency with which high and intermediate temperature finite thermal sources are utilized. The OFC's aim is to improve temperature matching and reduce exergy losses during heat addition. A theoretical investigation is conducted using high accuracy equations of state such as BACKONE, Span–Wagner, and REFPROP in a detailed thermodynamic and exergetic analysis. The study examines 10 different aromatic hydrocarbons and siloxanes as potential working fluids. Comparisons are drawn between the OFC and an optimized basic Organic Rankine Cycle (ORC), a zeotropic Rankine cycle using a binary ammonia-water mixture, and a transcritical CO_2 cycle. Results showed aromatic hydrocarbons to be the better suited working fluid for the ORC and OFC due to higher power output and less complex turbine designs. Results also showed that the single flash OFC achieves comparable utilization efficiencies to the optimized basic ORC. Although the OFC improved heat addition exergetic efficiency, this advantage was negated by irreversibilities introduced during flash evaporation. A number of potentially significant improvements to the OFC are possible though which includes using a secondary flash stage or replacing the throttling valve with a two-phase expander.

1. Introduction

As energy demands continue to rise, researchers continue to search for alternative energy sources to generate electricity, as well as improve existing methods to maximize efficiency. In order to meet global energy demands, a greater reliance on electricity generated from renewable energy sources such as solar thermal and geothermal energy will become necessary. For solar thermal, energy is obtained from a heated fluid circulating in a solar field, whereas for geothermal, energy is obtained from hot brine that has been extracted from a geothermal well. In addition to renewable sources, thermal energy that in the past would have been released and lost to the ambient such as hot exhaust exiting a gas turbine and industrial waste heat, are now being reexamined as potential power sources. These aforementioned energy sources are often termed as finite thermal energy reservoirs because the reservoir temperature and its thermal energy decreases dramatically as heat is transferred from the source to the power cycle. In order to make the most of these finite sources, the design of an efficient and effective power cycle is crucial.

One of the major sources of irreversibilities for vapor power cycles stems from the heat addition process. The thermal source and working fluid must be separated by some temperature difference in order for heat transfer to occur; however, heat transfer across a finite temperature difference inherently causes irreversibilities. Therefore, it is important to maintain good temperature matching between the heat exchanger streams to minimize these types of irreversibilities [1,2]. A large degree of temperature mismatching often does occur when the thermal source is single-phase and possesses a near linear temperature profile along the heat exchanger. For a vapor power cycle using a pure working fluid though, the working fluid is first heated as a liquid, undergoes liquid–vapor phase change, and if necessary, is further superheated as a vapor thereafter. Its temperature profile will first be near linear, then constant during phase change, and then near linear again, as shown in Fig. 1a. Temperature mismatching causes a pinch point to form, destroys potential work or exergy, and reduces the effectiveness of the heat exchangers [2]. To minimize temperature

* Corresponding author.
E-mail address: tony.ho@berkeley.edu (T. Ho).

0360-5442/$ – see front matter © 2012 Elsevier Ltd. All rights reserved.
doi:10.1016/j.energy.2012.03.067

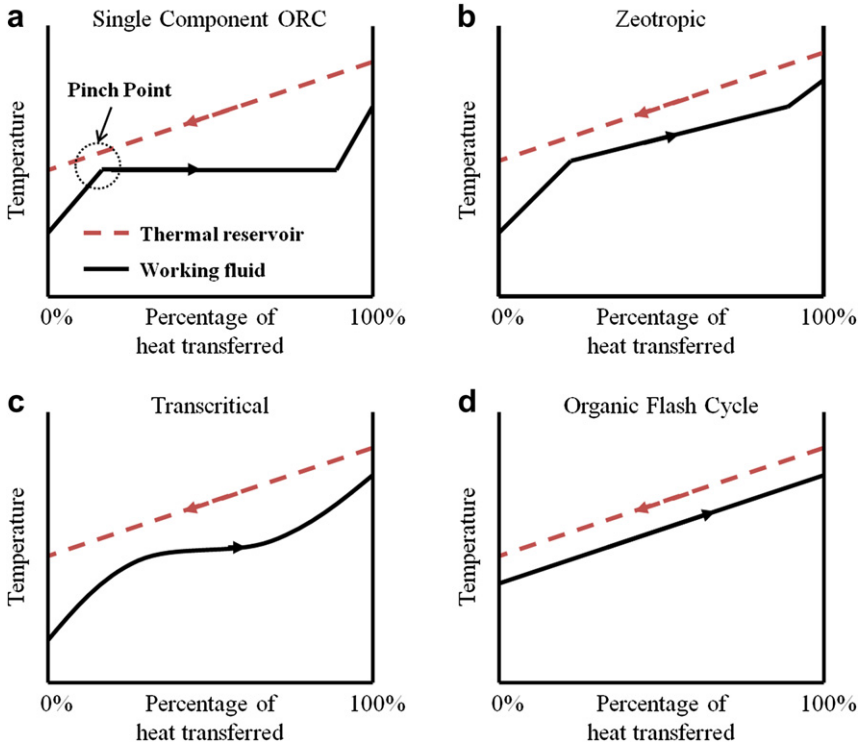

Fig. 1. Variation in stream temperatures during heat addition process for single component, zeotropic, transcritical and flash cycles [13].

mismatching, researchers have proposed a number of possible solutions that include utilizing unconventional working fluids and innovative cycle configurations and designs.

The use of zeotropic mixtures as working fluids in vapor cycles has been proposed by a number of researchers as a possible method to improve temperature matching [3–9]. Zeotropic mixtures exhibit a unique characteristic known as a "temperature glide," which results in a variation in temperature during isobaric phase change. Temperature gliding can produce a better temperature match to the finite thermal reservoir by avoiding isothermal phase change. As shown in Fig. 1b, the zeotropic working fluid's temperature glide follows the temperature profile of the thermal reservoir more closely. This reduces the irreversibilities in the heat addition process and can potentially improve the net power output and utilization efficiency [10].

Another method that has been suggested is to avoid the phase change region completely by transferring heat at pressures above the critical pressure [11–16]. This would essentially avoid the temperature mismatching encountered in the constant temperature phase change process. An illustration of the improved temperature matching is shown in Fig. 1c. A vapor cycle that operates partly under supercritical conditions is known as a transcritical cycle; working fluids that are often suggested for such cycles include carbon dioxide [13–15] and helium. Although theoretically the transcritical cycle has merit, the design of a suitable supercritical turbine for fluids other than water is still in the developmental phase [15]. A fluid under supercritical conditions can possess both liquid and vapor behaviors; thus tailoring a turbine specifically to one specific condition; i.e. liquid or vapor behavior, becomes problematic [17] and the development of an appropriate supercritical turbine design remains ongoing.

The trilateral flash cycle [17–20], another proposed method to improve temperature matching, faces similar challenges to that of the transcritical cycle. In the trilateral flash cycle, heat addition occurs while the working fluid is a single-phase liquid, thereby avoiding isothermal phase change as shown in Fig. 1d. Once the working fluid is heated to a saturated liquid state, work is then extracted using a two-phase expander. Similar to the transcritical cycle, the design of a reliable and efficient two-phase expander is still ongoing, though significant strides have been made recently for screw-type and scroll-type expanders and reciprocating engines [20]. To avoid the requirement of a two-phase expander though, the single-phase liquid could be throttled to a two-phase mixture after heat addition. The liquid and vapor components of the mixture can then be separated and work can be extracted from the saturated vapor using a conventional and readily available Organic Rankine Cycle (ORC) turbine. By using this type of configuration, a two-phase turbine is no longer necessary, while the advantageous temperature matching between streams shown in Fig. 1d is still achieved. This resulting cycle is somewhat similar to the flash steam cycle that utilizes high temperature and pressure geofluid that has been extracted in the liquid state from a geothermal well. Once extracted, the liquid geofluid is then throttled to a lower pressure or flashed to produce a liquid–vapor mixture [10]. One major disadvantage of the steam flash cycle though, is that the steam after expansion contains a significant amount of moisture because water is a "wet" fluid. Wet fluids exhibit a saturated vapor curve on a temperature-entropy (T-S) diagram that is negatively sloped [4]. Isentropic expansion of a "wet" fluid from its saturated vapor state will always produce a two-phase mixture with liquid droplets forming. Although in reality large steam turbines often have isentropic efficiencies of 80%–90%, saturated steam cycles in both geothermal and nuclear power industries still require special wet steam turbines. Wet steam turbines are constructed with expensive reinforcing materials to protect the blades from erosion and damage caused by the liquid droplets [10].

Expansion of a saturated vapor into the vapor dome can be avoided if a fluid with an infinite or positively sloped saturated vapor curve on a T-S diagram was used instead of steam [3]. These fluids are known as "isentropic" or "dry" fluids, respectively.

Turbine cost would be significantly reduced for the Organic Flash Cycle (OFC) since blade reinforcing materials are no longer necessary. Although uncontrolled expansion of the working fluid generates considerable irreversibilities during the throttling or flashing process [21], the reduction in exergy destruction during heat addition could still provide a net gain in the OFC's exergetic efficiency as a whole. The present study uses thermodynamic and exergetic analysis to evaluate the effectiveness of the OFC employing an organic "isentropic" or "dry" fluid. A finite thermal source originally at 300 °C is considered as it represents typical temperatures for high efficiency gas turbine exhaust, high temperature industrial waste heat or geothermal wells, and solar thermal energy using 1-axis tracking concentrated collectors such as parabolic troughs. Comparisons based on the internal second law efficiencies, heat addition exergetic efficiency, and utilization efficiency are then made to other vapor power cycles that have been proposed for solar thermal and waste heat applications.

2. Description of the Organic Flash Cycle

In Fig. 2a and b, a basic ORC plant layout and its T-S diagram are shown. Also shown are the T-S diagrams for a Rankine cycle using a zeotropic mixture and for a transcritical Rankine cycle. A schematic of the proposed OFC configuration and its T-S diagram are shown in Fig. 3a and b, respectively. Note that in Fig. 2 a "wet" fluid had been assumed, as the slope of the saturated vapor curve is negative, whereas in Fig. 3, a "dry" fluid has been assumed as the slope of the saturated vapor curve is positive. It can be seen from Fig. 3 that the OFC design is only slightly more complex than the basic Rankine cycle. The OFC cycle brings the saturated liquid working fluid at a low pressure at state 9 to a high pressure at state 1 as shown in Fig. 3 using a feed pump. In reality, state 9 would be slightly subcooled to prevent pump cavitation. Next, from states 1 to 2, the high pressure liquid absorbs heat from the finite thermal source and is then throttled, or flash evaporated, to a lower pressure liquid–vapor mixture at state 3. The mixture is separated into its saturated vapor and liquid components at states 4 and 6, respectively. From states 4 to 5, the saturated vapor is expanded to the condensing pressure and work is extracted. The saturated liquid is brought to the condenser pressure using a throttling valve from states 6 to 7. The liquid and vapor are then recombined in the mixer and then condensed back to a low pressure saturated liquid from states 8 to 9. It should be noted that energy in the saturated liquid can be further utilized by using an internal heat exchanger (IHE) as is often done in ORCs [4]. The flashing process could also be performed in two steps to extract more work; this is sometimes done in higher temperature geothermal plants to boost power output [10].

3. Methods of analysis

3.1. Equations of state explicit in Helmholtz energy

To determine the thermodynamic properties of different working fluids, accurate equations of state are necessary. Since increases in efficiency by even just a few percent is important, simple equations of state such as cubic ones do not possess enough accuracy for analysis in this study. Instead a combination of modern equations of state such as the semi-empirical BACKONE equations [22,23], the empirical, multi-parameter Span–Wagner equations [24–27], and the equations of state compiled in REFPROP 8.0 [28] were employed to determine thermodynamic states and properties. The BACKONE and Span–Wagner equations of state are explicit in Helmholtz energy and are functions of density and temperature; they can also be cast into the general form shown in Eq. (1) [24],

$$\frac{a(T,\rho)}{RT} = \alpha(T,\rho) = \alpha^0 + \alpha^R \tag{1}$$

where a is the Helmholtz free energy, R is the universal gas constant, T is temperature, ρ is density, and α, α^0, and α^R are the total, ideal gas component, and residual component of the reduced Helmholtz energy.

The ideal gas portion of the reduced Helmholtz energy is well known and given in Eq. (2) [24,29],

$$a^0 = \frac{h^0_{\mathrm{ref}}\tau}{RT_0} - 1 + \ln\left(\frac{\delta\tau_{\mathrm{ref}}}{\delta_{\mathrm{ref}}\tau}\right) - \frac{s^0_{\mathrm{ref}}}{R} - \frac{\tau}{R}\int_{\tau_{\mathrm{ref}}}^{\tau}\frac{c^0_p}{\tau^2}d\tau + \frac{1}{R}\int_{\tau_{\mathrm{ref}}}^{\tau}\frac{c^0_p}{\tau}d\tau \tag{2}$$

where h is enthalpy, s is entropy, the subscript ref denotes the property at an arbitrary reference state, and c^0_p is the ideal gas isobaric heat capacity, which can be determined theoretically from statistical thermodynamics or, as was done in this study, it can be approximated using power law correlations that are available for a number of fluids in Ref. [25–27,30]. τ and δ are inverse reduced temperature and reduced density and are given in Eq. (3),

$$\tau = T_0/T; \quad \delta = \rho/\rho_0 \tag{3}$$

where T_0 and ρ_0 are a fluid specific characteristic temperature and density. The residual portion of the reduced Helmholtz energy can be cast in the general form shown in Eq. (4),

$$\alpha^R(\tau,\rho) = \sum_{i=1}^{I_{\mathrm{pol}}} n_i\tau^{t_i}\delta^{d_i} + \sum_{i=I_{\mathrm{pol}}+1}^{I_{\mathrm{pol}}+I_{\mathrm{exp}}} n_i\tau^{t_i}\delta^{d_i}\exp\left(-g_i\delta^{p_i}\right) \tag{4}$$

where n_i, t_i, d_i, g_i, and p_i are constants dependent on the specific Helmholtz-explicit equation of state selected and I_{pol} and I_{exp} are

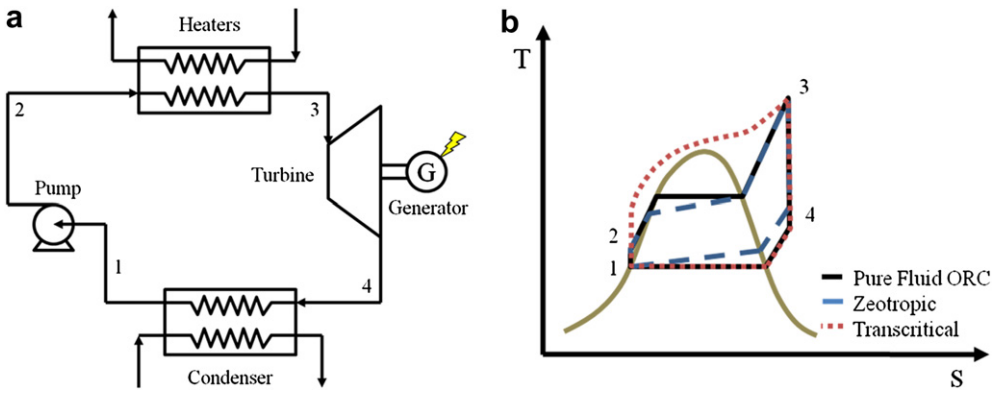

Fig. 2. Plant schematic and T-S diagram for basic pure fluid ORC, zeotropic Rankine cycle, and transcritical Rankine cycle.

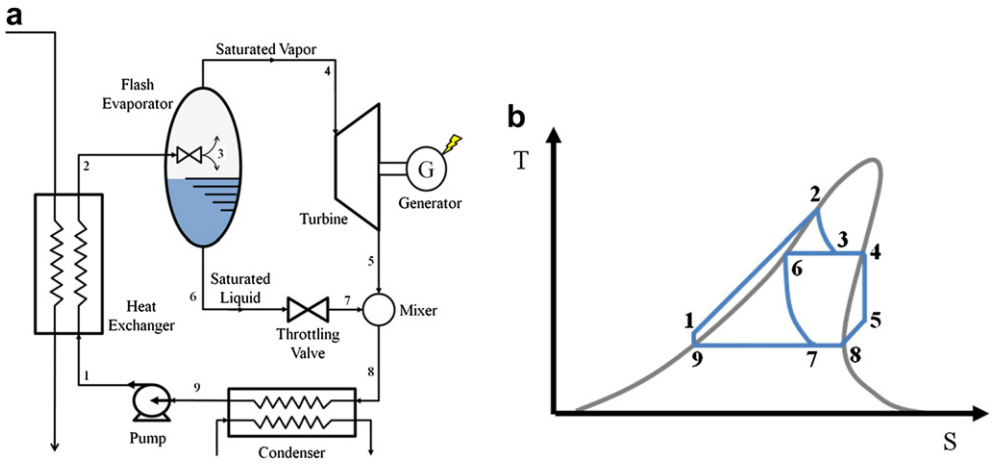

Fig. 3. Plant schematic and T-S diagram for single flash OFC.

the number of polynomial and exponential terms, respectively [24]. The BACKONE equations are termed semi-empirical as they possess some theoretical basis to the residual contribution. For the BACKONE equations, the residual contribution is further split into contributions from the hard body repulsive forces using perturbation theories, the attractive-dispersive intermolecular forces for nonpolar molecules, and a term accounting for dipolar or quadrupolar interactions for polar molecules [22–24]. The Span–Wagner equations are empirical multi-parameter equations of state that utilize optimized empirical data to determine the coefficients in Eq. (4) [24–27].

Thermodynamic properties such as pressure, enthalpy, entropy, etc. can be determined directly from a combination of temperature, density, Helmholtz energy, and partial derivatives of Helmholtz energy with respect to temperature and/or density. The derivations of these and other thermodynamic properties are covered in great detail in Ref. [24]. Due to the Helmholtz energy being defined in terms of its natural variables of density and temperature, determining thermodynamic states from other combinations of properties such as temperature and pressure or pressure and enthalpy requires complicated iterative procedures. Examples of some of the iterative techniques often used are also discussed in Ref. [24]. For the working fluids considered in this study, the authors verified the calculated vapor pressure and saturated liquid and vapor density values from the BACKONE and Span–Wagner equations by comparing with values given on the online NIST Chemistry WebBook [31]. For the conditions of interest, excellent agreement was obtained between the NIST data tables and the equations of state utilized in this study. The BACKONE and Span–Wagner equations of state have also been utilized in several other advanced vapor cycle studies in the literature [32–34].

Besides the BACKONE and Span–Wagner equations, NIST REFPROP 8.0 is also utilized in this study. In REFPROP 8.0, thermodynamic properties can be calculated for a large number of refrigerants and hydrocarbons typically used in combustion and refrigeration processes. Depending on the selected working fluid, the program will either apply an equation of state explicit in Helmholtz energy, the modified Benedict–Webb–Rubin equation of state, or an Extended Corresponding States (ECS) model [28]. The equations of states utilized in REFPROP are all highly accurate and have been incorporated in other ORC investigations in the literature as well [2,3,35]. EES is also another often used computational tool that compiles equations of state for ORC design and other technical applications [13,14].

3.2. Thermodynamic and exergetic analysis

One thermodynamic property that is particularly useful in power analysis is potential work or exergy χ, defined in Eq. (5),

$$\chi = h - T_d s \tag{5}$$

where the subscript d designates the property at the dead state [21]. The dead state in this study is taken to be the conditions of the ambient environment. Two parameters that are often used to determine power cycle effectiveness are the first law and internal second law efficiencies defined in Eqs. (6) and (7) respectively,

$$\eta_I = W_{\text{net}}/Q_{\text{add}} \tag{6}$$

$$\eta_{II,\text{int}} = \frac{W_{\text{net}}}{\dot{m}_f\left(\chi_{f,\text{out}} - \chi_{f,\text{in}}\right)} \tag{7}$$

where W_{net} is the net power produced by the cycle, Q_{add} is the heat transfer rate during the heat addition process, $\dot{m}_f$ is the working fluid flow rate, and $\chi_{f,\text{in}}$ and $\chi_{f,\text{out}}$ are the working fluid exergy before and after heat addition, respectively. From Eqs. (6) and (7), it is noted that η_I is the ratio of net work produced to the heat added, whereas $\eta_{II,\text{int}}$ is the ratio of the net work produced to the potential work added. However these parameters do not completely quantify how well a cycle performs in applications such as waste heat reclamation or as a bottoming cycle for high temperature solar thermal if the energy in the thermal energy source stream is discarded or unused. This unused exergy in the source stream is known as “lost exergy” [16]. In applications where the energy from the source stream is not used further after transferring heat to the power cycle, the primary objective is to maximize the amount of heat transferred to the power cycle from the source stream and simultaneously maximize the power produced from this transferred energy. The 1st law and internal 2nd law efficiencies, however, only consider how efficient the cycle is with respect to producing work from a given amount of energy or exergy that it absorbs. These parameters do not consider how effective the cycle is at absorbing the energy or exergy from the thermal source. Therefore, a power cycle could have very high 1st and internal 2nd law efficiencies, but produce little power because not much energy is absorbed from the thermal source. In some applications such as combined heat and power, energy in the finite thermal heat source needs to be used conservatively because it is to be used further after

transferring heat to the power cycle. In such a case, the efficiency parameter of primary interest is the external 2nd law efficiency shown in Eq. (8); note this efficiency is similar to the internal 2nd law efficiency but it also accounts for the exergy destruction due to heat transfer across a finite temperature difference from the source to the power cycle.

$$\eta_{II,\text{ext}} = \frac{W_{\text{net}}}{\dot{m}_s(\chi_{s,\text{in}} - \chi_{s,\text{out}})} \tag{8}$$

In many waste heat applications though, where energy left in the source stream is discarded or unused after heat is transferred to the vapor cycle, a more appropriate parameter is the utilization efficiency ε, defined in Eq. (9) [10,16,36,37],

$$\varepsilon = \frac{W_{\text{net}}}{\dot{m}_s(\chi_{s,\text{in}} - \chi_{s,d})} \tag{9}$$

where $\dot{m}_s$ represents the source flow rate, $\chi_{s,\text{in}}$ is the source's inlet exergy, and $\chi_{s,d}$ is the source's exergy at the dead state. Note that in defining the utilization efficiency in Eq. (9), the source's exergy at the dead state is used rather than the source's exergy at the exit of the heat exchanger. This parameter is appropriate when assuming that after the source stream has transferred heat to the vapor cycle for power production, whatever remaining exergy from the source stream goes unused and is eventually lost to the environment. This is often the case for waste heat and bottoming cycles. Although theoretically another cycle could be applied, practically this secondary cycle would not be cost-effective with respect to either the capital cost to install it or the power produced because the source stream to this cycle would be at such a low temperature. For solar thermal applications, it is also useful to return the solar heat transfer fluid to the solar field as close to ambient temperatures as possible to reduce heat losses in the receiver thus achieving high receiver efficiencies which contributes to the overall system efficiency. The utilization efficiency is a ratio of how much power is produced to the amount of work theoretically possible from a given finite thermal source. In this study, the utilization efficiency parameter can also be thought of as a nondimensional parameter for power as the same energy source with some initial exergy will be specified. Note this definition of utilization efficiency is the product of the internal 2nd law efficiency $\eta_{II,\text{int}}$ and the heat addition exergetic efficiency η_{add} as shown in Eq. (10),

$$\varepsilon = \frac{W_{\text{net}}}{\dot{m}_s(\chi_{s,\text{in}} - \chi_{s,d})} = \left[\frac{W_{\text{net}}}{\dot{m}_f(\chi_{f,\text{out}} - \chi_{f,\text{in}})}\right]\left[\frac{\dot{m}_f(\chi_{f,\text{out}} - \chi_{f,\text{in}})}{\dot{m}_s(\chi_{s,\text{in}} - \chi_{s,d})}\right] = \eta_{II}\eta_{\text{add}} \tag{10}$$

where the subscript *f*,in and *f*,out designate the working fluid at its inlet and outlet of the heat exchanger. Utilization efficiency is maximized when the system is efficient at both absorbing energy from the finite thermal source as well as converting it to useful work.

A number of simplifying assumptions that are used in power plant analysis have been employed in this study [21]. Frictional losses in the piping and heat exchanger have been considered small and negligible; the heat addition and condensing processes are therefore assumed to be isobaric. Changes in the working fluid's kinetic and potential energies have also been considered negligible. The steady flow devices in the vapor cycle are all considered to be well insulated and do not lose significant energy to the surroundings. Throttling valves are assumed to be isenthalpic devices [10,21]. Mixing chambers and separators are assumed to be isobaric, adiabatic, and have no work interactions [21]. The turbine and feed pump are assumed to deviate from ideal isentropic behavior by isentropic efficiencies of η_{turb} and η_{pump}, respectively. The construction of energy balances across different steady flow devices is well known and the details can be found in Refs. [21,38]. A computational program was constructed in MATLAB to model a variety of different working fluids for the OFC. An analysis is made to compare the internal and external second law, utilization, and heat addition exergetic efficiencies of the OFC to those obtained for optimized basic ORC and an ammonia-water zeotropic Rankine cycle [5,8,9,39] and to a CO_2 transcritical cycle [13–15], two of the more often suggested power cycles in the literature.

4. Results and discussion

4.1. Results for the basic ORC

Aromatic hydrocarbon and siloxane working fluids have often been proposed for ORCs utilizing a high or intermediate temperature finite thermal source [6,32,40,41]. A list of the fluids analyzed in this study has been compiled in Table 1, along with the equation of state that was used and its corresponding references. Note in Table 1, aromatic hydrocarbons are first listed and then siloxanes. The finite thermal source is modeled as hot water initially at 300 °C flowing at a steady rate of 1 kg/s. The ambient temperature is assumed to be 30 °C and a minimum pinch temperature difference of at least 10 °C in the heat exchanger is assumed necessary to facilitate heat transfer between the two streams. Based on Carnot considerations, the temperature of the working fluid at the condenser outlet is set to the ambient temperature plus the pinch (40 °C) in both the ORC and OFC. Isentropic efficiencies of 85% are assumed for the feed pumps and turbines. Design parameters of the basic ORC include the turbine inlet temperature and pressure and the working fluid flow rate. Therefore to maximize the utilization efficiency and power production, ORC optimization is required with respect to both the turbine inlet temperature and pressure and the corresponding maximum flow rate that would still yield a minimum 10 °C temperature difference between streams during heat addition.

Using a toluene working fluid as an example, Fig. 4 shows the utilization efficiency as a function of the turbine inlet pressure ratio

Table 1
List of working fluids analyzed for OFC, ORC, zeotropic, and transcritical vapor cycles.

Fluid name	Vapor cycle	T_{crit} [K]	Equation of state and reference
Toluene	OFC/ORC	591.75	REFPROP [28]
Ethylbenzene	OFC/ORC	617.20	BACKONE [22,23,32]
Butylbenzene	OFC/ORC	660.05	BACKONE [22,23,32]
o-xylene	OFC/ORC	630.33	BACKONE [22,23,32]
m-xylene	OFC/ORC	617.05	BACKONE [22,23,32]
p-xylene	OFC/ORC	616.23	BACKONE [22,23,32]
Tetradecamethylhexasiloxane (MD4M)	OFC/ORC	653.2	Span–Wagner [24–27]
Decamethylcyclopentasiloxane (D5)	OFC/ORC	619.2	Span–Wagner [24–27]
Dodecamethylpentasiloxane (MD3M)	OFC/ORC	628.36	Span–Wagner [24–27]
Dodecamethylcyclohexasiloxane (D6)	OFC/ORC	645.78	Span–Wagner [24–27]
0.7/0.3 ammonia-water (NH_3-H_2O)	Zeotropic	505.82	REFPROP [28]
Carbon dioxide (CO_2)	Transcritical	304.13	REFPROP [28]

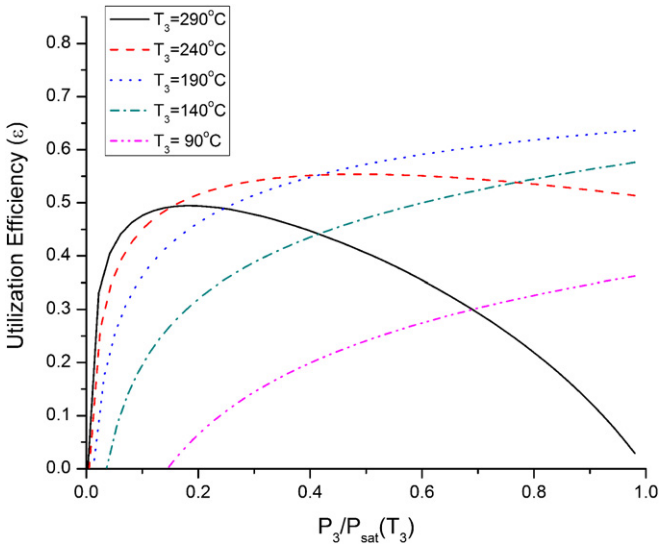

Fig. 4. Utilization efficiency for a basic toluene ORC for varying turbine inlet temperature and pressure.

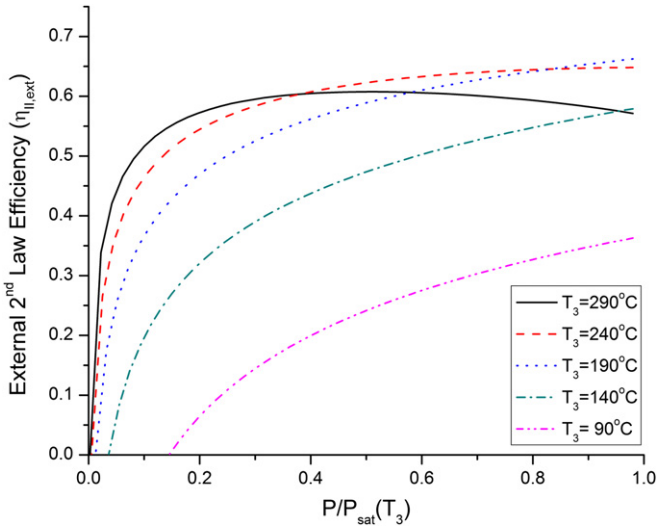

Fig. 5. External 2nd law efficiencies for a basic toluene ORC for varying turbine inlet temperature and pressure.

for several turbine inlet temperatures. As shown in Fig. 4, the utilization efficiency is strongly dependent on both the inlet turbine temperature and pressure at state 3 of Fig. 2. Depending on the turbine inlet temperature, the shape of the utilization efficiency curve is vastly different. At a 290 °C turbine inlet temperature, the maximum utilization efficiency is reached when the fluid is significantly superheated at state 3. At higher pressures, little power is produced from the thermal energy source because poor heat addition exergy efficiencies are encountered, which are a result of poor temperature matching, low cycle flow rate, and little energy being transferred to the ORC. For turbine inlet temperatures of 240 °C and 190 °C, one sees that the maximum of the utilization efficiency curves in Fig. 4 begin to increase and shift towards the right. Utilization efficiency actually increases with lower turbine inlet temperature because state point 3 is becoming less superheated and consequently, state point 4 at the turbine exit is less superheated and heat rejection occurs at a lower temperature which increases the internal 2nd law efficiency. High superheat at the turbine exit is a particular concern for "dry" working fluids as they tend to have significant superheat after expansion through a turbine because of their positively sloped saturated vapor curve on a T-S diagram. As the turbine inlet temperature is further decreased to 140 °C and 90 °C, the curves maintain the same shape, but the maximum of the curves begin to decrease. The average heat addition temperature is now approaching the average heat rejection temperature of the cycle and poor efficiency results based on Carnot considerations. These general trends just described were observed for all the working fluids in this study. For the fluids considered, because they are "dry" fluids, the maximum utilization efficiency was achieved at an inlet turbine temperature significantly below the initial temperature of the heat source.

As noted previously, the utilization efficiency is the appropriate efficiency parameter for situations in which the finite thermal energy source stream is not used further after transferring heat to the power cycle [16,36,37]. In some cases though, the heat source stream is valuable and useful for applications such as providing building heat; in such a scenario, the more appropriate parameter becomes the external 2nd law efficiency because energy left in the source stream will still be used in a different application. Using a toluene working fluid as an example again, Fig. 5 shows the external 2nd law efficiency as a function of turbine inlet pressure ratio for several turbine inlet temperatures. Note that the general behavior of the curves is very similar to that of Fig. 4, and the preceding observations on the trends in Fig. 4 are also applicable to Fig. 5. In the present study, the basic ORC was optimized to maximize either utilization efficiency or external 2nd law efficiency; the thermodynamic state at point 3 and corresponding cycle mass flow rate for the ORC optimized to both variables are shown in Table 2. Also given in Table 2 is the pressure at state 1 for the basic ORC; note this state also corresponds to state 9 of the OFC as well. Table 2 shows that for some of the working fluids considered, the turbine inlet conditions for maximum utilization efficiency and maximum external 2nd law efficiency do not correspond. Assuming a saturated vapor at the turbine inlet, Fig. 6 shows the external 2nd law efficiencies and corresponding utilization efficiency or nondimensional power output. For aromatic hydrocarbons, Fig. 6 shows that there are a range of potential turbine inlet conditions where there is a balance between maximizing power generation and external 2nd law efficiency. This is shown specifically for toluene by the top right quadrant formed by the dotted vertical and horizontal lines indicating maximum utilization efficiency and internal 2nd law efficiency respectively. The balance between maximizing efficiency and power generation is well known in the field of endoreversible and finite time thermodynamics and further discussion on this topic can be found in Ref. [42].

Table 2
Thermodynamic states for key points and mass flow rates of the optimized ORC.

Fluid name	P_1[a] [kPa]	Optimized to ε		Optimized to $\eta_{II,ext}$	
		T_3[b] [K]	$\dot{m}_{ORC}$ [kg/s]	T_3[b] [K]	$\dot{m}_{ORC}$ [kg/s]
Toluene	7.867	454	1.69	478	1.44
Ethylbenzene	2.852	451	1.72	476	1.45
Butylbenzene	0.3965	452	1.74	468	1.55
o-xylene	2.302	455	1.60	468	1.47
m-xylene	2.506	453	1.67	471	1.48
p-xylene	2.621	454	1.68	468	1.53
MD4M	0.0050	509	2.31	504	2.35
D5	0.0771	506	2.47	499	2.54
MD3M	0.0237	508	2.28	503	2.33
D6	0.0125	509	2.45	505	2.50

[a] $P_1 = P_{sat}(T_1 = 40\ ^\circ C)$, also corresponds to OFC at $P_9 = P_{sat}(T_9 = 40\ ^\circ C)$ as a saturated liquid.
[b] State point 3 is a saturated vapor ($q_3 = 1$) for the ORC optimized to either ε or $\eta_{II,ext}$.

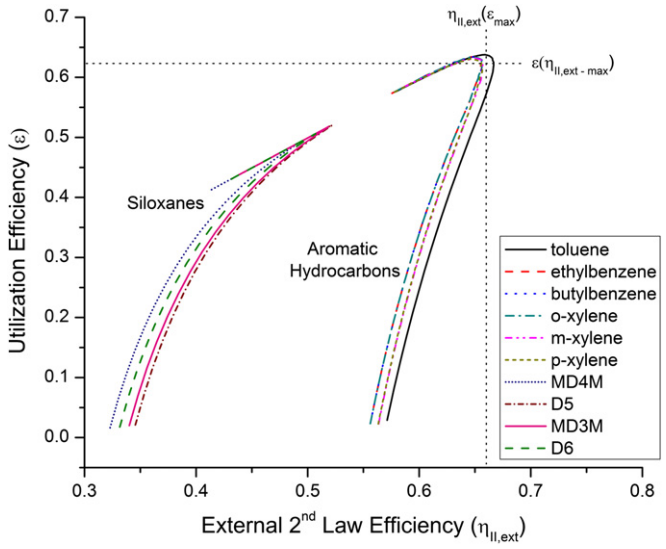

Fig. 6. Utilization efficiency versus external 2nd law efficiency for basic ORC at a saturated vapor state at turbine inlet.

Fig. 7 shows utilization efficiency as a function of the ratio of the turbine inlet pressure to the fluid saturation pressure at the temperature for maximum utilization efficiency as given in Table 2. Note again for all the curves, utilization efficiency and thus power generation, reaches a maximum when the working fluid is at a saturated vapor state at the turbine inlet. Fig. 7 shows that aromatic hydrocarbons achieved significantly higher utilization efficiencies than siloxanes. This difference in performance can be attributed in large part to the molecular structure of siloxanes as compared to aromatic hydrocarbons. Using a statistical thermodynamics argument, Tabor and Bronicki [43] showed that more complex molecules exhibit a more "drying" behavior and possess a less positively sloped saturated vapor curve on a T-S diagram. Siloxanes are more complex and thus exhibit more "drying" behavior. After expansion from a saturated vapor state, siloxanes will then be at a higher temperature and superheated to a greater degree than their aromatic hydrocarbon counterparts. However, in the basic ORC this high temperature, superheated vapor with considerable exergy is simply cooled in the condenser and the potential work it possessed is not utilized. Some ORC studies have suggested an internal heat exchanger (IHE) to reuse energy from the turbine exhaust to preheat the fluid leaving the feed pumps [4,32]. This improves the internal 2nd law efficiency since the amount of energy absorbed from the external source is reduced, while the net work produced remains constant. However, an IHE does not improve the utilization efficiency or maximum power generation [36,44]. This is because the exergetic efficiency of the heat addition process decreases as a result of less energy being transferred from the finite thermal source, and energy from the source that is not utilized is calculated as wasted potential work or "lost exergy" [16]. However, the IHE does improve the external 2nd law efficiency because even though less energy from the heat source stream is transferred to the power cycle, the power cycle is not penalized for this because it is assumed that the remaining energy will be used in the next application. This difference in usefulness of an IHE again points to the importance of identifying the context with which the vapor power cycle is to be operated in so that the appropriate efficiency parameter is used in the design and analysis of the power cycle.

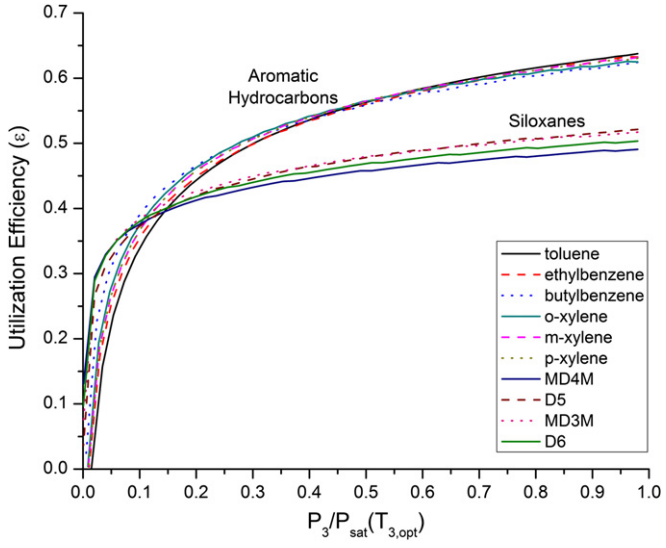

Fig. 7. Utilization efficiency for basic ORC at varying inlet turbine pressures and T_3 from Table 2 for a particular working fluid.

4.2. Results for the OFC

The OFC cycle analysis begins with determining the optimal state for the fluid to be throttled to so that the utilization efficiency is maximized. This is done in concert with determining the temperature at the inlet of the flash evaporator and its corresponding maximum flow rate that still provides the minimum 10 °C temperature difference between streams of the heat exchanger. Through some simplifications, DiPippo determined analytically the optimal state using the "equal-temperature-split rule" [10]. Here, an iterative method is employed to determine the optimal state with which to flash the fluid to. Table 3 gives, for maximum utilization efficiency, some important thermodynamic states for the OFC including state 3, the state the fluid should be flash evaporated to. Fig. 8 shows a plot of the resulting maximum utilization efficiencies for the OFC and the percentage difference compared to the maximum utilization efficiency for the optimized ORC determined earlier in Fig. 7. Fig. 8 shows the OFC to exhibit comparable performance to the optimized ORC in terms of the utilization efficiency, with the OFC generating about 0%–2.5% less power than the optimized ORC. Results show that the advantages resulting from increasing the exergetic efficiency during the heat addition process to be comparable to the disadvantages of introducing the throttling process in flash evaporation and the added irreversibilities that it generates. The exergetic efficiency of the heat addition process for the optimized ORC averaged ~75% for aromatic hydrocarbons,

Table 3
Optimal thermodynamic state 3 to flash evaporate to for the OFC in terms of temperature T_3 and vapor mass quality q_3 and corresponding cycle mass flow rate.

Fluid name	T_2[a] [K]	T_3 [K]	q_3	$\dot{m}_{OFC}$ [kg/s]
Toluene	559	457	0.87	1.92
Ethylbenzene	561	453	0.89	1.90
Butylbenzene	563	452	0.94	1.85
o-xylene	562	452	0.86	1.90
m-xylene	561	453	0.87	1.92
p-xylene	561	453	0.87	1.93
MD4M	557	507	1.00	2.31
D5	558	509	1.00	2.43
MD3M	552	502	1.00	2.33
D6	557	507	1.00	2.46

[a] State point 2 for the optimized OFC is a saturated liquid ($q_2 = 0$).

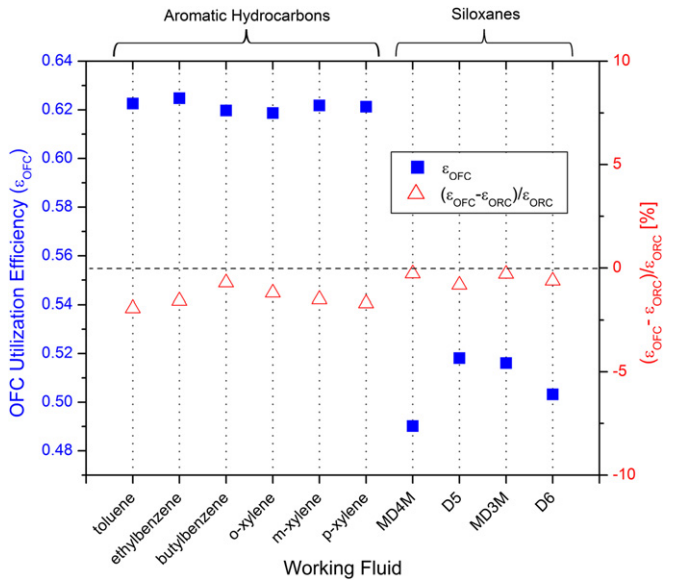

Fig. 8. OFC utilization efficiencies and the percent difference in utilization efficiency for OFCs compared to the optimized ORC.

whereas for siloxanes it neared 89%. This high heat addition exergetic efficiency for siloxanes can be attributed to their molecular complexity which gives siloxane molecules many degrees of freedom and in turn makes the specific heat for siloxanes very high. Their high specific heat causes the majority of the heat that is absorbed in the cycle to go towards heating the siloxane from a subcooled state at the pump exit (state 1) to a saturated liquid state. The energy required to vaporize the siloxane working fluid is actually fairly small compared to the necessary sensible heat; this is actually advantageous in the ORC as it allows the siloxane temperature profile to match that of the energy source fairly well resulting in high heat addition exergetic efficiency. Unfortunately, as mentioned previously, their molecular complexity also makes the fluid very "drying;" this contributes to very high superheat at the turbine exit and low internal 2nd law efficiencies which then limits the total power generated. This is the primary reason why aromatic hydrocarbons, which are less "drying," exhibited better performance than siloxanes for the OFC, as shown in Fig. 8. For the OFC, the heat addition exergetic efficiency for aromatic hydrocarbons was slightly over 90%, approximately a 20% improvement over the optimized ORC. For siloxanes in the OFC, the heat addition exergetic efficiency was approximately 92%, which only amounts to about a 3% improvement over the optimized ORC.

In addition to power output, practical considerations such as the design of a suitable turbine or expander should be taken into consideration when selecting a working fluid. Neglecting Reynolds number effects, Macchi et al. [45] used similarity arguments to show that the efficiency of a particular turbine stage can be approximated quite well from the Volumetric Flow Ratio (VFR) and the Size Parameter (SP) which are defined in Eqs. (11) and (12), respectively [45].

$$\mathrm{VFR} = \left(\dot{V}_{\mathrm{out}}/\dot{V}_{\mathrm{in}}\right)_{\mathrm{isen}} \tag{11}$$

$$\mathrm{SP} = \sqrt{\dot{V}_{\mathrm{out}}}/(\Delta h)^{0.25}_{\mathrm{isen}} \tag{12}$$

In Eqs. (11) and (12), $\dot{V}_{\mathrm{out}}$ and $\dot{V}_{\mathrm{in}}$ are the volumetric flow rates at the turbine stage exit and inlet, Δh is the enthalpy drop across the stage, and the subscript isen denotes an isentropic process. VFR is essentially the turbine expansion ratio and can also be thought of as a compressibility parameter; SP is a dimensional parameter which is an approximate indication of the turbine's actual size [45,46]. Table 4 gives the VFR and SP for the optimized ORC and OFC for the working fluids considered. For single stage axial turbines, isentropic efficiencies of at least 80% are only possible for a VFW below ~50 [46,47]. Note that for all the working fluids in this study, the VFW was determined to be above this threshold; this indicates that an axial turbine of at least 2 stages would be necessary to achieve the isentropic efficiencies of 85% which had been assumed in this study. Siloxanes in particular have VFRs from 2 to 3 orders of magnitude greater than aromatic hydrocarbon working fluids indicating that multiple stages beyond 2 stages would likely be necessary in order to achieve reasonable isentropic efficiencies. In addition, MD4M and D6 have very high VFRs compared to all the other working fluids. When considering the high cost of multi-stage turbines, using these working fluids may not actually be cost justified in practice. Note in Table 4 that the SP and VFR are very similar between the optimized ORC and OFC; this would confirm that turbine technology already available for the ORC are also likely suitable for the OFC.

4.3. Potential improvements for the OFC

Fig. 8 shows that the single flash OFC exhibits only comparable utilization efficiencies to the optimized ORC; however, there are a number of potential improvements that could raise the OFC utilization efficiency considerably. One method could be to use two separate flash steps instead of only one, similar to the double flash steam cycle that is applied to higher temperature geothermal resources [10]. This double flash OFC would also then have two turbines, one high pressure turbine for saturated vapor from the first flash step, and then a second low pressure turbine for vapor gathered from the secondary flash step. Introducing a secondary flash step reduces the irreversibilities associated with the flash evaporation process; for geothermal resources, double flash steam cycles have reported 15%–20% more power generated compared to a single flash steam cycle for the same geofluid. Another potential improvement could be to replace the throttling valve with a two-phase expander; this concept has been discussed and is of a particular interest in the refrigeration and oil refining industries. Replacing the throttling valve with a two-phase expander would significantly improve the OFC, as a previous source of irreversibility has now become a source of power generation. Reheat loops using the liquid from the first flash step for aromatic hydrocarbons or reverse feedwater heaters to reduce vapor superheat at the turbine exit for siloxanes are also potential areas for improvement.

Table 4
Turbine Size Parameter (SP) and Volumetric Flow Ratio (VFR) for conditions for optimized ORC and OFC.

Fluid Name	OFC		ORC optimized to ε		ORC optimized to $\eta_{II,\mathrm{ext}}$	
	SP [m]	VFR	SP [m]	VFR	SP [m]	VFR
Toluene	0.132	62.1	0.133	58.4	0.120	93.7
Ethylbenzene	0.210	86.9	0.212	83.2	0.191	140
Butylbenzene	0.522	197	0.522	198	0.487	291
o-xylene	0.242	96.8	0.239	104	0.233	137
m-xylene	0.221	91.8	0.221	91.2	0.205	135
p-xylene	0.217	88.8	0.217	90.8	0.205	122
MD4M	3.70	1.09×10^4	3.70	1.15×10^4	3.73	1.01×10^4
D5	1.06	2.39×10^3	1.07	2.23×10^3	1.09	1.89×10^3
MD3M	1.82	4.20×10^3	1.80	4.87×10^3	1.82	4.31×10^3
D6	2.46	6.23×10^3	2.46	6.55×10^3	2.49	5.93×10^3

4.4. Comparing the OFC with other proposed cycles

A variety of modifications to the basic ORC have been proposed by researchers to improve temperature matching, heat addition exergetic efficiency, and system utilization efficiency. Two frequently suggested approaches are employing binary mixtures or operating the cycle partly supercritical. An analysis was conducted to compare the performance of the proposed OFC to that for a basic ammonia-water Rankine cycle and a basic transcritical CO_2 Rankine cycle.

4.4.1. Comparing the OFC to a basic ammonia-water Rankine cycle

For comparison, a basic Rankine cycle using an ammonia-water mixture 0.70/0.30 mass ratio was analyzed. This particular zeotropic fluid is chosen because it is the mixture that is used in the widely known Kalina cycle. Fig. 9 shows the exergetic efficiency of the heat addition process, the internal 2nd law efficiency, and the utilization efficiency for the ammonia-water Rankine cycle as a function of the expansion ratio (P_3/P_4) and turbine inlet pressure (P_3). Only conditions that produced vapor qualities greater than or equal to 0.85 after expansion have been presented, as too much moisture would erode and damage the steam turbine blades [48]. Note that for the ammonia-water Rankine cycle which utilizes a "wet" fluid, the turbine inlet temperature is set to the maximum 290 °C. This was done to ensure that at higher boiler pressures, the mixture is still superheated enough at the turbine inlet to avoid expansion into the vapor dome at the turbine exit.

Fig. 9 shows that the zeotropic ammonia-water Rankine cycle achieves comparable heat addition exergetic efficiency to the optimized ORC at about 75%. The temperature glide exhibited by zeotropic fluids has been shown here to not noticeably improve temperature matching during heat addition compared to the optimized ORC. This result, however, may be due to a poor selection of mixture concentration; a detailed design of a zeotropic cycle would select concentration ratios and mixtures such that it matches the temperature profile of the energy source very closely. From Fig. 9, the maximum utilization efficiency obtained was only about 0.46, which is considerably below that obtained for the optimized ORC. The low utilization efficiency can be attributed to the same temperature glide property researchers exploit to improve heat addition efficiency. After expansion, zeotropic fluids are at a much higher temperature than their pure fluid counterparts because of the temperature glide. The high temperature, high exergetic content of the exhaust stream is then lost in the condenser. Similar results were seen by Wang et al. [4] for a low temperature solar ORC. Their results showed that the pure fluid R245fa ORC outperformed ORCs using three different zeotropic mixtures of R245fa/R152a. The Kalina cycle attempts to reclaim this exergy by using a distiller-condenser-subsystem (DCSS), which changes the working fluid composition multiple times in different loops [39,46]. By incorporating the DCSS, some have claimed that the Kalina cycle improves efficiency by 10%–50% over the conventional steam Rankine cycle depending on the temperature of the thermal reservoir [49]. However, others have noted the increase in efficiency to be closer to about 3% [50]. Fig. 9 shows yet another major obstacle for an ammonia-water Rankine cycle is the high operating pressures. Care must be taken to select the proper fluids and concentration ratio to ensure better temperature matching, as well as reducing the disadvantages of the temperature glide during the condensing process.

4.4.2. Comparing the OFC to the transcritical CO_2 cycle

Operating the Rankine cycle partially in the supercritical regime is another method that researchers have suggested to improve temperature matching. CO_2 is often cited as a working fluid for such a cycle due to its inexpensiveness, availability, and stability [13–15]. Performance parameters for a simple transcritical CO_2 Rankine cycle are plotted in Fig. 10. Note that for the CO_2 cycle, the assumed cold thermal reservoir temperature is reduced to 20 °C from 30 °C, which had been used in the analysis of all the preceding cycles thus far. The temperature reduction of the cold thermal reservoir is necessary to achieve subcritical condensing of CO_2.

From Fig. 10, the heat addition exergetic efficiency for the transcritical CO_2 cycle is observed to be about 75%–80%. This increase in exergetic efficiency compared to the optimized ORC is again due to supercritical heating that avoids isothermal phase change that occurs in the two-phase region. By adding heat to CO_2 above the critical pressure, better temperature matching to the

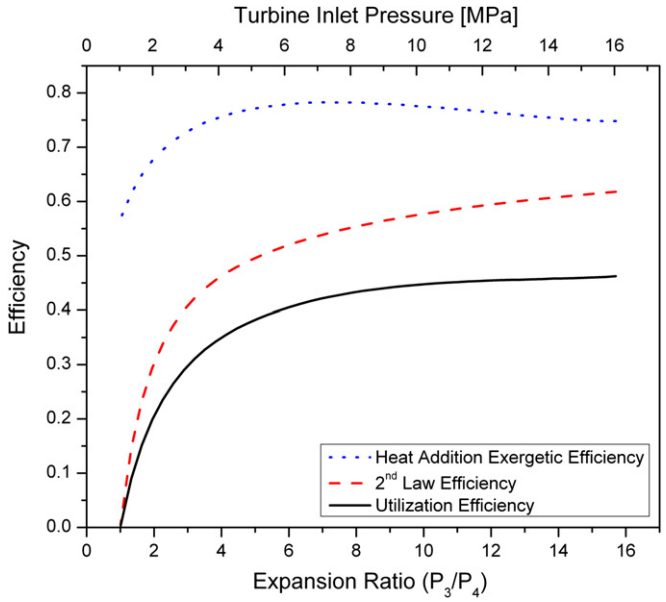

Fig. 9. Performance parameters for a zeotropic ammonia-water Rankine cycle (0.70/0.30 by mass).

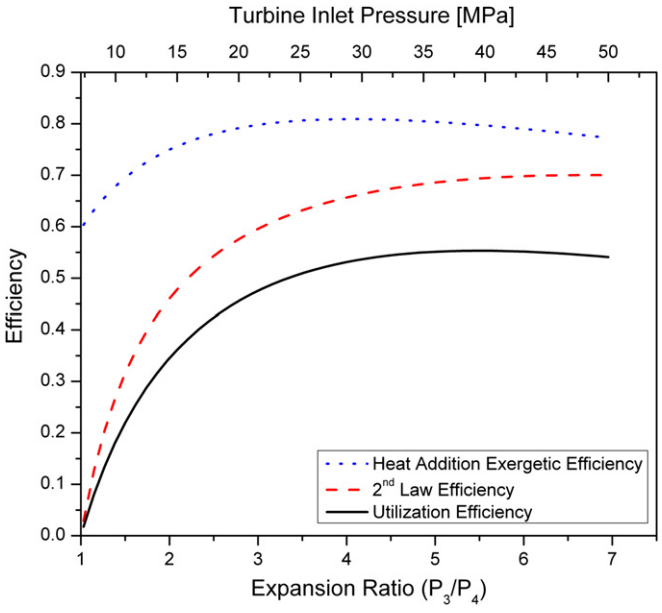

Fig. 10. Performance parameters for a transcritical CO_2 Rankine cycle.

finite thermal source is achieved. Although the exergetic efficiency of the heat addition process is slightly higher for the transcritical CO_2 cycle compared to the optimized ORC, it should be noted that it is still less than the greater than 90% exergetic efficiency achieved by the OFC. In this study, the maximum utilization efficiency achieved by the simple transcritical CO_2 cycle was about 0.55, which is about 13% less than the maximum achieved by the OFC and optimized ORC, 0.62 and 0.63, respectively. Similar to the ammonia-water Rankine cycle, very high operating pressures are encountered for a transcritical CO_2 cycle, as shown in Fig. 10. The OFC and optimized ORC on the other hand are both completely subcritical and thus operate under much lower pressures. Yet another obstacle for the transcritical CO_2 cycle is the aforementioned design of a suitable supercritical CO_2 turbine which is still under development [15].

5. Conclusions

A comparison of the Organic Flash Cycle to the optimized ORC and other advanced vapor cycles for high and intermediate temperature finite thermal sources was presented. The OFC concept is based upon the design principle of increasing utilization efficiency by increasing temperature matching and reducing exergy losses during the heat addition process. REFPROP, BACKONE, and Span–Wagner equations of states were used in conjunction with a detailed thermodynamic and exergetic analysis to determine the validity and merit of the OFC. A number of different aromatic hydrocarbons and siloxanes were analyzed as potential working fluids. For the working fluids examined, results showed the OFC to have comparable performance to the optimized ORC. Aromatic hydrocarbons were shown to outperform siloxanes as working fluids for both the OFC and optimized ORC. While the OFC also possessed the highest heat addition exergetic efficiency of the cycles analyzed, this advantage was negated by the exergy destruction introduced by the throttling valve in the flash evaporation process. However, a number of improvements are possible for the OFC that could significantly increase net power generation. Research into these potential improvements to OFC is warranted due to the significant potential gains in efficiency and the possible applications to lower temperature thermal energy sources.

Nomenclature

a	Helmholtz free energy [J/kg]
c_p	isobaric heat capacity [J/kg K]
d_i, g_i, n_i, p_i, t_i,	equation of state specific constants
h	enthalpy [J/kg]
I_{exp}	number of exponential terms in equation of state
I_{pol}	number of polynomial terms in equation of state
$\dot{m}$	mass flow rate [kg/s]
q	vapor quality
Q_{add}	heat addition [W]
R	ideal gas constant (8.314 J/mol K)
s	entropy [J/kg]
SP	Size Parameter [m]
T	temperature [K]
T_0	fluid specific characteristic temperature [K]
$\dot{V}$	volumetric flow rate [m^3/s]
VFR	Volumetric Flow Ratio
W_{net}	net power [W]

Greek symbols

α	total reduced Helmholtz energy
α^0	ideal gas component of Helmholtz energy
α^R	residual component of Helmholtz energy
δ	reduced density
ε	utilization efficiency
$\eta_{II,int}$	internal 2nd law efficiency
$\eta_{II,ext}$	external 2nd law efficiency
η_{add}	heat addition exergetic efficiency
ρ_0	fluid specific characteristic density [kg/m^3]
τ	inverse reduced temperature
χ	exergy [J/kg]

Subscripts and superscripts

d	dead state
f	fluid
in	inlet
l	liquid
out	outlet
ref	reference
s	source
sat	saturated
v	vapor

References

[1] Vargas JVC, Bejan A. Thermodynamic optimization of the match between two streams with phase change. Energy 2000;25:15–33.
[2] Venkatarathnam G, Mokashi G, Murthy SS. Occurrence of pinch points in condensers and evaporators for zeotropic refrigerant mixtures. International Journal of Refrigeration 1996;19:361–8.
[3] Wang JL, Zhao L, Wang XD. A comparative study of pure and zeotropic mixtures in low-temperature solar Rankine cycle. Applied Energy 2010;87:3366–73.
[4] Wang XD, Zhao L. Analysis of zeotropic mixtures used in low-temperature solar Rankine cycles for power generation. Solar Energy 2009;83:605–13.
[5] Murugan RS, Subbarao PMV. Thermodynamic analysis of Rankine-Kalina combined cycle. International Journal of Thermodynamics 2008;11:133–41.
[6] Angelino G, Di Paliano PC. Multicomponent working fluids for organic Rankine cycles (ORCs). Energy 1997;23:449–63.
[7] Wu C. Non-azeotropic mixture energy conversion. Energy Conversion and Management 1985;25:199–206.
[8] Lolos PA, Rogdakis ED. A Kalina power cycle driven by renewable energy sources. Energy 2009;34:457–64.
[9] Ibrahim OM, Klein SA. Absorption power cycles. Energy 1996;21:21–7.
[10] DiPippo R. Geothermal power plants: principles, applications, and case studies. Oxford: Elsevier; 2005.
[11] Chen H, Goswami DY, Rahman MM, Steanakos EK. A supercritical Rankine cycle using zeotropic mixture working fluids for the conversion of low-grade heat into power. Energy 2010;36:549–55.
[12] Gu Z, Sato H. Performance of supercritical cycles for geothermal binary design. Energy Conversion and Management 2002;43:961–71.
[13] Cayer E, Galanis N, Desilets M, Nesreddine H, Roy P. Analysis of a carbon dioxide transcritical power cycle using a low temperature source. Applied Energy 2009;86:1055–63.
[14] Chen Y, Lundqvist P, Johansson A, Platell P. A comparative study of the carbon dioxide transcritical power cycle compared with an organic Rankine cycle with R123 as working fluid in waste heat recovery. Applied Thermal Engineering 2006;26:2142–7.
[15] Zhang XR, Yamaguchi H, Fujima K, Enomoto M, Sawada N. Study of solar energy powered transcritical cycle using supercritical carbon dioxide. International Journal of Energy Research 2006;30:1117–29.
[16] Schuster A, Karellas S, Aumann R. Efficiency optimization potential in supercritical organic Rankine cycles. Energy 2008;35:1033–9.
[17] Smith IK. Development of the trilateral flash cycle system part 1: fundamental considerations. Proceedings of the Institution of Mechanical Engineers, Part A: Journal of Power and Energy 1993;207:179–94.
[18] Zamfirescu C, Dincer I. Thermodynamic analysis of a novel ammonia-water trilateral Rankine cycle. Thermochimica Acta 2008;477:7–15.
[19] Crook AW. Profiting from low-grade heat: thermodynamic cycles for low-temperature heat sources. Glasgow: Institution of Electrical Engineers; 1994.
[20] Fischer J. Comparison of trilateral cycles and organic Rankine cycles. Energy 2011;36:6207–19.
[21] Cengel YA. Thermodynamics: an engineering approach. 5th ed. Boston: McGraw Hill; 2006.
[22] Muller A, Winkelmann J, Fischer J. BACKONE family of equations of state: 1. Nonpolar and polar pure fluids. AIChE Journal 1996;42:1116–26.

[23] Weingerl U, Wendland M, Fischer J, Muller A, Winkelmann J. BACKONE family of equations of state: 2. Nonpolar and polar fluid mixtures. AIChe Journal 2001;47:705–17.
[24] Span R. Multiparameter equations of state: an accurate source of thermodynamic property data. Berlin: Springer; 2000.
[25] Lemmon EW, Span R. Short fundamental equations of state for 20 industrial fluids. Journal of Chemical Engineerng Data 2006;51:785–850.
[26] Colonna P, Nannan NR, Guardone A, Lemmon EW. Multiparameter equations of state for selected siloxanes. Fluid Phase Equilibria 2006;244:193–211.
[27] Colonna P, Nannan NR, Guardone A. Multiparameter equations of state for siloxanes: $[(CH_3)_3\text{-}Si\text{-}O_{1/2}]_2\text{-}[O\text{-}Si\text{-}(CH_3)_2]_{i=1,3,}$ and $[O\text{-}Si\text{-}(CH_3)_2]_6$. Fluid Phase Equilibria 2008;263:115–30.
[28] Lemmon EW, Huber ML, McLinden MO. NIST standard reference database 23: reference fluid thermodynamic and transport properties – REFPROP version 8.0. Gaithersburg: National Institute of Standards and Technology, Standard Reference Data Program; 2010.
[29] Jacobsen RT, Lemmon EW, Penoncello SG, Shan Z, Wright NT. Thermophysical properties of fluids and materials. In: Bejan A, Kraus A, editors. Heat transfer handbook. Hoboken: John Wiley & Sons Inc; 2003. p. 40–163.
[30] Reid RC, Prausnitz JM, Poling BE. The properties of Gases and liquids. 4th ed. New York: McGraw-Hill Book Company; 1987.
[31] Linstrom PJ, Mallard WG, editors. NIST Chemistry WebBook, NIST standard reference database number 69. Gaithersburg: National Institute of Standards and technology. http://webbook.nist.gov. [retrieved December 15, 2011].
[32] Lai NA, Wendland M, Fischer J. Working fluids for high-temperature organic Rankine cycles. Energy 2011;36:199–211.
[33] Saleh B, Koglbauer G, Wendland M, Fischer J. Working fluids for low-temperature organic Rankine cycles. Energy 2007;32:1210–21.
[34] Fernández FJ, Prieto MM, Suárez I. Thermodynamic analysis of high-temperature regenerative organic Rankine cycles using siloxanes as working fluids. Energy 2011;36:5239–49.
[35] Desai NB, Bandyopadhyay S. Process integration of organic Rankine cycle. Energy 2009;34:1674–86.
[36] Dai Y, Wang J, Gao L. Parametric optimization and comparative study of organic Rankine cycle (ORC) for low grade waste heat recovery. Energy Conversion and Management 2009;50:576–82.
[37] Galanis N, Cayer E, Roy P, Denis ES, Désilets M. Electricity generation from low temperature sources. Journal of Applied Fluid Mechanics 2009;2:55–67.
[38] Moran MJ, Shapiro HN. Fundamentals of engineering thermodynamics. 5th ed. Hoboken: John Wiley & Sons Inc.; 2004.
[39] Zhang YM, He M, Jai Z, Liu X. First law-based thermodynamic analysis on Kalina cycle. Frontiers of Energy and Power in China 2008;2:145–51.
[40] Saavedra I, Bruno JC, Coronas A. Thermodynamic optimization of organic Rankine cycles at several condensing temperatures: case study of waste heat recovery in a natural gas compressor station. Proceedings of the Institution of Mechanical Engineers, Part A: Journal of Power and Energy 2010;224:917–30.
[41] Colonna P, Guardone A, Nannan NR. Siloxanes: a new class of candidate Bethe-Zel'dovich-Thompson fluids. AIP Physics of Fluids 2007;19:086102.
[42] Chen J, Yan Z, Lin G, Andresen B. On the Curzon-Ahlborn efficiency and its connection with the efficiencies of real heat engines. Energy Conversion and Management 2001;42:173–81.
[43] Tabor H, Bronicki L. Establishing criteria for fluids for small vapor turbines. SAE Transactions 1965;73:561–75.
[44] Quoilin S, Declaye S, Lemort V. Expansion machine and fluid selection for the organic Rankine cycle. In. 7th international conference on heat transfer, fluid mechanics and thermodynamics. Antalya, Turkey; 19–21 July 2010.
[45] Macchi E, Perdichizzi A. Efficiency prediction for axial-flow turbines operating with nonconventional fluids. ASME Journal of Engineering for Power 1981; 103:718–24.
[46] Invernizzi C, Iora P, Silva P. Bottoming micro-Rankine cycles for micro-gas turbines. Applied Thermal Engineering 2007;27:100–10.
[47] Angelino G, Invernizzi C, Macchi E. Organic working fluid optimization for space power cycles. In: Angelino G, DeLuca L, Sirignano WA, editors. Modern Research Topics in aerospace propoulsion. New York: Springer-Verlag; 1991.
[48] Li KW, Priddy AP. Power plant system design. New York: John Wiley & Sons; 1985.
[49] Mlcak HA. An introduction to the Kalina cycle. In. Proceedings of the international joint power generation conference; 30 1996. ASME International Book No H01077. p. 1–11.
[50] Chen H, Goswami DY, Stefanakos EK. A review of thermodynamic cycles and working fluids for the conversion of low-grade heat. Renewable and Sustainable Energy Reviews 2010;14:3059–67.